



UNIVERSITY OF LEEDS

This is a repository copy of *A two-step synthesis for preparing metal microcapsules with a biodegradable polymer substrate*.

White Rose Research Online URL for this paper:
<http://eprints.whiterose.ac.uk/130050/>

Version: Accepted Version

Article:

Tasker, AL, Puttick, S, Hitchcock, J orcid.org/0000-0003-2226-6734 et al. (4 more authors) (2018) A two-step synthesis for preparing metal microcapsules with a biodegradable polymer substrate. *Journal of Materials Chemistry B*, 6 (14). pp. 2151-2158. ISSN 2050-750X

<https://doi.org/10.1039/c8tb00348c>

(c) The Royal Society of Chemistry 2018. This is an author produced version of a paper published in *Journal of Materials Chemistry B*. Uploaded in accordance with the publisher's self-archiving policy.

Reuse

Items deposited in White Rose Research Online are protected by copyright, with all rights reserved unless indicated otherwise. They may be downloaded and/or printed for private study, or other acts as permitted by national copyright laws. The publisher or other rights holders may allow further reproduction and re-use of the full text version. This is indicated by the licence information on the White Rose Research Online record for the item.

Takedown

If you consider content in White Rose Research Online to be in breach of UK law, please notify us by emailing eprints@whiterose.ac.uk including the URL of the record and the reason for the withdrawal request.



eprints@whiterose.ac.uk
<https://eprints.whiterose.ac.uk/>

A Two-step Synthesis for Preparing Metal Microcapsules with a Biodegradable Polymer Substrate

Alison L. Tasker^{1,2,3*}, Simon Puttick^{2,3}, James Hitchcock⁴, Olivier J. Cayre⁴, Idriss Blakey², Andrew K. Whittaker^{2,5}, Simon Biggs⁶

1. School of Chemical Engineering, University of Queensland, St. Lucia, Queensland, 4072, Australia.
2. Australian Institute of Bioengineering and Nanotechnology, University of Queensland, St. Lucia, Queensland, 4072, Australia.
3. CSIRO Probing Biosystems Future Science Platform
4. School of Chemical and Process Engineering, University of Leeds, Leeds, LS2 9JT, UK
5. ARC Centre of Excellence in Convergent Bio-Nano Science and Technology, University of Queensland, St Lucia, 4072
6. Faculty of Engineering, Architecture and Information Technology, University of Queensland, St. Lucia, Queensland, 4072, Australia.

[*a.tasker@uq.edu.au](mailto:a.tasker@uq.edu.au)

Abstract

Metal microcapsules have recently received attention and are being developed as improved carrier materials when compared to polymer microcapsules. In this work we have developed a novel, simplified method by which polymeric microcapsules can be synthesised using a combination of poly(vinyl pyrrolidone)-stabilised platinum nanoparticles (PVP-Pt) and poly(vinyl pyrrolidone) (PVP) as stabilisers, to allow for a secondary metal shell to be grown. We investigate the relationship between the molar ratio of reducing agent to platinum salt and the size of the resulting NPs and seek to develop further fundamental understanding of the factors governing the secondary metal shell thickness and quality, to allow production of cost-effective metal microcapsules without sacrificing core retention efficiency. We found that the size of the nanoparticles had no significant effect on secondary shell thickness, but did affect the quality of the resulting gold shells. Gold salt concentration was found to be a limiting factor in the electroless deposition of the metal shell. In this work, we have successfully produced PLGA microcapsules with more cost-effective gold shells, as thin as 56 ± 13 nm and capable of complete core retention of volatile actives.

Introduction

Encapsulation of active compounds within polymeric shells has been explored over many decades and has led to the development of a vast array of applications including foods,¹ pharmaceuticals,²⁻⁵ inks,⁶⁻⁸ homecare⁹⁻¹¹ and personal care products.^{12, 13} However, there is an inherent disadvantage in using polymers as the shell material: due to the relatively high permeability of the polymer matrix, low molecular weight volatile actives can easily escape through the shell, particularly in environments which favour leakage, such as a bulk solvent in which the active is highly soluble.

Improving the retention of small molecules in the microcapsule core has therefore been a major focus in the literature for decades.¹⁴⁻¹⁸ Increasing the thickness of the polymer shell,^{14, 15} polymer cross linking,¹⁹ and changing the solvent used in the bulk phase,¹⁷ are just some of the methods which have been employed in an attempt to improve the active's retention time. Such approaches however, do not actually prevent leakage and only serve to lower the rate of release, in many cases only slowing complete loss by a few hours. Alternative approaches, such as the use of fluorinated monomers to form the polymer shell, prevents wetting of the shell and showed significant improvement in retarding the diffusion of molecules from the core.¹⁷ However, this is unlikely to be a practical solution as such a method for producing a fluorinated shell is currently only achievable via microfluidic production and the use of fluorinated monomers as the middle oil phase of a multiple emulsion is likely to be challenging to translate into a scalable batch process. Recently, metal films have been demonstrated as a potential shell material, allowing for complete retention of volatile molecules within microcapsules.^{16, 20, 21} For example, in our previous work, we demonstrated that hexyl salicylate is fully retained within a metal-shell microcapsule for at least 21 days at elevated temperatures when exposed to a bulk ethanol:water phase in which it is fully soluble.¹⁶

The metal-shell microcapsules reported in our earlier work were prepared in a three step synthesis involving synthesis of polymer shell microcapsules from an emulsion template, using the solvent extraction method first described by Loxley and Vincent.^{14, 15, 22} Platinum nanoparticles, stabilised with poly(vinyl pyrrolidone) (PVP-Pt) were then physically adsorbed onto this polymer shell and finally, the adsorbed nanoparticles acted as catalytic loci for the growth of a continuous gold shell by electroless deposition, in stage three.²³ As this method uses precious metals, platinum and gold, to form the metal shells, it is imperative that

adequate control is gained for both nanoparticle adsorption and the subsequent gold shell formation, to allow for thin, continuous shells to be produced thus lowering production costs.

Whilst this method has shown promise, it was found to be challenging to control the physical adsorption of PVP-Pt nanoparticles onto the polymer microcapsule surface in some cases. For example, we demonstrated that the adsorption of nanoparticles has some dependence on the material present in the core.²¹ Based on these observations and various attempts to grow a controlled gold shell of a desired thickness we were able to propose mechanisms which describe the growth of the gold shells, depending on the deposition and density of the metal nanoparticles adsorbed onto the polymer surface.²¹ It was postulated that when nanoparticle aggregation occurred on the surface of the capsule, forming multiple layers of nanoparticles, that the gold shell would grow in such a way that it filled the gaps in the nanoparticle framework. Thus, in order to grow the thinnest and most cost-effective shells, better control of the nanoparticle density is required, to prevent aggregation and to give a dense monolayer on the polymer surface. In the work reported here, we have improved on our previous method by directly utilising the metal nanoparticles as a stabiliser for the initial capsule formation, as described in the work of Cayre and Biggs.²⁴ This method results in catalytic nanoparticles anchored onto the polymer surface as the shell is formed potentially allowing greater control over the distribution of the nanoparticles on the microcapsule surface.

There is much work in the literature relating to the use of the biodegradable and biocompatible polymer poly(d,l-lactide-co-glycolic acid) (PLGA) as a microcapsule shell to encapsulate the ultrasound contrast agent perfluorooctyl bromide (PFOB).²⁵⁻²⁸ These capsules are formed using a similar solvent extraction method to the one we have described previously.^{16,22} In contrast to our previous work however, polymeric stabilisers such as poly(vinyl alcohol) (PVA) and poly(vinyl pyrrolidone) (PVP) are used to form small, spherical core-shell capsules.²⁵ The addition of an impermeable gold shell to such biocompatible microcapsules could allow, not only for improved stability of ultrasound contrast agents, but also for improved drug delivery, potentially eliminating off-target side effects as the drug cannot leach from the capsules prior to controlled or deliberate breakage.

In this work, we aim to stabilise such PLGA microcapsules with a PFOB core using PVP-Pt nanoparticles, in combination with an excess of PVP, to achieve a uniform monolayer of nanoparticles embedded securely on the capsule surface, allowing us to then control the

growth of a complete, and potentially thinner, gold shell directly onto the capsules by electroless deposition.

Materials

Poly(lactic-co-glycolic acid), (PLGA), (50:50) (10-15 kDa), dichloromethane, (DCM); poly(vinyl pyrrolidone) (PVP) (40 kDa); chloroplatinic acid, (H_2PtCl_6) 99%; chloroauric acid (HAuCl_4) 99.99%; perfluorooctyl bromide, (PFOB); 30% hydrogen peroxide (H_2O_2); poly(ethylene glycol) (PEG) (400 Da); chloroform-D (CDCl_3) 99.8%; pentafluorobenzyl alcohol 98%; and sodium borohydride (NaBH_4) 98%, were purchase from Sigma Aldrich. All chemicals were used as received.

Preparation of PLGA microcapsules with embedded Pt nanoparticles.

First, PVP-stabilised Pt nanoparticles were synthesised. H_2PtCl_6 (0.115g, 2.2 mM) was dissolved in 100 mL of PVP solution (1.15 μM). In a 250 mL conical flask the H_2PtCl_6 solution was stirred vigorously and NaBH_4 (0.4 mL, 0.5 M) was rapidly injected into the flask. The yellow solution immediately turned dark brown, and after two minutes of vigorous stirring was left to stand for at least 12 hours to form an almost black nanoparticle dispersion of PVP-Pt. To investigate the effect of nanoparticle size on the final metal shell thickness, H_2PtCl_6 concentrations of 0.5, 1.1, 2.2, 3.3 and 4.4 mM were used. PVP-Pt dispersions were concentrated by dialysis in PEG400 solution (5 wt%) to remove any excess water., to achieve a constant number concentration of nanoparticles across all samples,

PLGA (0.1 g) was dissolved in DCM (4 mL) before PFOB (60 μL) was added and mixed until a single phase was formed. PVP (2.0 g) was dissolved into 100 mL ultrapure water (18.2 $\text{M}\Omega\text{ cm}$ at 25 $^\circ\text{C}$) to form part of the continuous phase. To the PVP solution (15 mL), PVP-Pt nanoparticles (5 mL) were added. The oil-in-water emulsion was formed by slowly adding this aqueous solution onto the PLGA-PFOB phase and then emulsifying (IKA T25 Ultra-Turrax) at 17500 rpm for 2 min, over ice. The emulsion was stirred at 300 rpm for 24 hours to allow complete evaporation of the DCM and precipitation of the polymer shell. The capsules were washed twice via centrifugation at 2000 rpm for 10 minutes at 10 $^\circ\text{C}$ followed by redispersion in 25 mL ultrapure water.

Metal shell growth onto PLGA microcapsules.

A gold plating solution was prepared consisting of HAuCl_4 (1.0 mL, 40 mM), PVP (3.0 mL, 0.05 mM) and H_2O_2 (1.0 mL, 60 mM). To this, a PLGA capsule dispersion (0.5 mL) was added dropwise, then mixed on a carousel for 5 minutes at 50 rpm. The capsules were washed

three times via centrifugation at 2000 rpm for 2 minutes at room temperature, and redispersed in 5 mL ultra pure water with 0.2 mL PVP (0.05 mM) as a stabiliser to prevent aggregation. To investigate the effect of concentration of HAuCl_4 on the resulting metal shell thickness, the salt concentration was reduced to 30 mM, 20 mM, 10 mM and 5 mM, while all other parameters remained constant.

Characterisation of nanoparticles

Size distributions of the Pt nanoparticles were measured using transmission electron microscopy, TEM (JEOL1010) at 80 kV and the micrographs were analysed using the analyse particles function in ImageJ, image analysis software (imageJ.net)²⁹. At least 600 particles were measured for each sample. Polydispersity was measured from the ratio of the quadratic average. To calculate the number of nanoparticles synthesised in each sample, UV-vis spectroscopy was used to measure the conversion of H_2PtCl_6 to Pt^0 . The absorbance of the H_2PtCl_6 peak was measured at 244 nm, and used to calculate the Pt^0 concentration. Using this and the nanoparticle size data we calculated the number of nanoparticles synthesised.

Characterisation of nanoparticle distribution on PLGA microcapsules

To measure the nanoparticle distribution on a capsule surface, transmission electron microscopy, TEM (JEOL1010) at 80 kV was used to collect images of collapsed (and thus transparent) capsules. The nanoparticle coverage was measured as a percentage using ImageJ, image analysis software.

Characterisation of metal shells

Scanning electron microscopy, SEM (Hitachi SU3500) was used to observe the gold shell morphology. A Zeiss Field emission SEM (FE SEM) with Gatan 3View was used to take multiple cross sections through the metal capsules, set in an epoxy resin, then ImageJ was used to measure the thickness of the metal shells in each slice to find the mid-point of each capsule and thus the point where the metal shell appears thinnest, representing the true shell thickness. This method is based on our previous work where microtome slices were analysed using TEM and ImageJ to calculate shell thickness.¹⁶ In addition, to remove experimenter bias, shell thickness was determined using a MATLAB code developed in-house. Briefly, single capsules were isolated manually and then segmented based on a global image mean. The resulting binary image was subjected to a Euclidean distance transform and the centre of the shell wall identified by selecting pixels with the maximum distance from the background in an 8-connected component neighbourhood. The shell thickness was taken as twice the

average distance (the number of measurements for each shell in each slice was greater than 100) from the centre pixel to the background. To gain a statistical representation of the capsule population, the measurements were repeated for each slice for 20 full capsules.

To test for leakage from the core, samples of microcapsules with gold or polymer shells were added to CDCl_3 (2 mL) with a pentafluorobenzyl alcohol marker (5 mg/mL), and mixed on a disk tube rotator (MX-RD-E, Scilogex USA) for 7 days. The solutions were filtered to remove any remaining capsules and then ^{19}F NMR was used to detect the presence of PFOB in the filtrate.

Results and discussion

PVP-Pt nanoparticles as a stabiliser in the formation of PLGA-PFOB microcapsules

The aim of this part of the work was to investigate the potential of using PVP-Pt nanoparticles to stabilise PLGA microcapsule formation, to allow better control over the distribution of nanoparticles on the capsule surface. Seekell et al. have shown previously that it is possible to form PLGA shell-PFOB core microcapsules when PVP is utilised as the stabiliser, using the solvent evaporation method.³⁰ As the Pt nanoparticles used to catalyse gold deposition in previous works are also stabilised with PVP,^{16, 21, 23} we hypothesised that PVP-Pt could be used to stabilise the PLGA-PFOB microcapsules. However, platinum is an expensive, precious metal and thus using large amounts would be undesirable when considering scale up for industrial translation. Therefore we used a combination of pure PVP and PVP-Pt to stabilise the capsules thus minimising the amount of platinum required to stabilise the interface, whilst ensuring enough PVP-Pt coverage to allow secondary metal shell growth. We hypothesised that the PVP-Pt nanoparticles would act as a synergistic stabiliser to the PVP, and that we could gain more control of the nanoparticle coverage on the microcapsule surface, in turn allowing further control of the final gold shell thickness.²¹

We found that spherical core-shell microcapsules were indeed formed using this combination of PVP and PVP-Pt, as predicted from the spreading coefficients of the capsule components, described in our previous work (Table S1 supplementary information).¹² The resulting emulsion is shown in Figure 1a) where a schematic representation and optical microscope image of an emulsion droplet is displayed. As the solvent evaporates, the polymer becomes insoluble in the remaining oil and migrates to the oil-water interface, eventually forming a shell around the PFOB core once there is no DCM remaining. The nanoparticles which were

used to stabilise the emulsion become trapped on the capsule surface during the shell formation, and this can clearly be seen in Figure 1b (schematic and transmission electron micrograph). The nanoparticles appear evenly distributed across the polymer surface in a single monolayer. This is in contrast to what is observed when physically adsorbing PVP-Pt with an excess of PVP to pre-formed polymer shells, where the PVP and the PVP-Pt compete for space on the solid surface.³¹ Continuous gold shells are grown onto the platinum embedded microcapsules by electroless deposition, using the procedure previously described,^{16, 21} and the resulting gold shell can be seen in Figure 1c (schematic and scanning electron micrograph). Release of PFOB from the capsules was tested using ¹⁹F NMR. PFOB was detected in the solvent phase for the capsules with a polymer shell, which indicated that either the polymer shell had dissolved or the PFOB had diffused through the shell. On the other hand, no PFOB signal was observed in the solvent phase for the gold coated capsules (Figure S1), indicating full retention of the core.

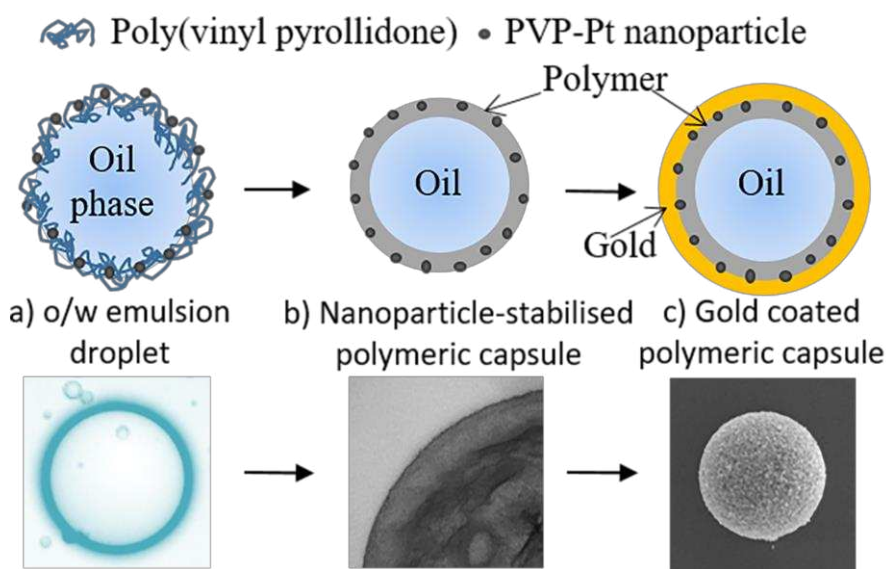
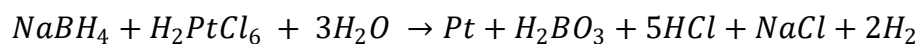


Figure 1 – Schematic diagram of metal microcapsule formation, with microscopy images of each stage a) PVP and PVP-Pt stabilised emulsion droplet with corresponding optical microscopy image, b) solvent evaporation results in polymer precipitation to form a shell around the PFOB, trapping the nanoparticles at the surface, demonstrated in transmission electron micrograph, c) resulting gold shell with corresponding scanning electron micrograph. Images chosen are representative of the sample and chosen specifically to highlight each stage of the procedure.

The reduction of H_2PtCl_6 to $\text{Pt}^{(0)}$ proceeds as shown in Equation (1). The metal salt is reduced by sodium borohydride to produce the platinum nanoparticles in the presence of PVP, which acts as a stabiliser for the nanoparticles. Due to the low concentration of PVP used in the synthesis, the nanoparticles formed were at the limit of stability, as described in our previous work,²¹ and so if more platinum salt was reduced, there were insufficient PVP chains available to stabilise the additional nanoparticles, leading to aggregation and sedimentation of

platinum (Figure S2). Thus, the mass of platinum salt was reduced to investigate the effect of the molar ratio of $\text{NaBH}_4:\text{H}_2\text{PtCl}_6$ on the formation of the platinum nanoparticles. UV-Vis spectroscopy was used to calculate the concentration of $\text{Pt}^{(0)}$ formed in the reaction, from the absorbance measured at 244 nm, and this is shown in Figure 2a.



Equation (1)

Transmission electron micrographs of the nanoparticles demonstrate that for a molar ratio above 1:1 $\text{NaBH}_4:\text{H}_2\text{PtCl}_6$ the nanoparticles do not form aggregates (Figure 3).

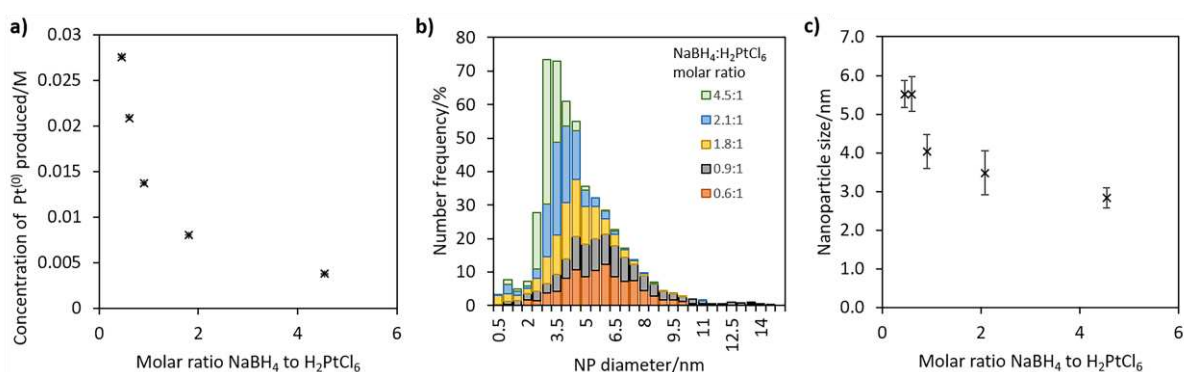


Figure 2 – Effect of molar ratio of $\text{NaBH}_4:\text{H}_2\text{PtCl}_6$ used in PVP-Pt synthesis on a) resulting Pt concentration, b) size distribution of NPs produced, and c) median nanoparticle size.

It is also clear from Figure 2b that the mean nanoparticle size reduces as the molar ratio of reducing agent to platinum salt is increased. The nanoparticle size was measured from transmission electron micrographs of the nanoparticles and analysed using the image analysis software, ImageJ. The dispersity can be seen to increase as the molar ratio of $\text{NaBH}_4:\text{H}_2\text{PtCl}_6$ is reduced, as indicated in Figure 2b, where the normalised number frequency distribution for each sample is shown. There is an increased availability of PVP per unit nanoparticle surface area when the platinum salt concentration is reduced (increasing the ratio of reducing agent to platinum salt), leading to more uniformity of the nanoparticles. This is also evidenced in Figure 3, where the TEM images show that with increasing platinum salt and thus decreasing molar ratio, the resulting nanoparticles are noticeably larger.

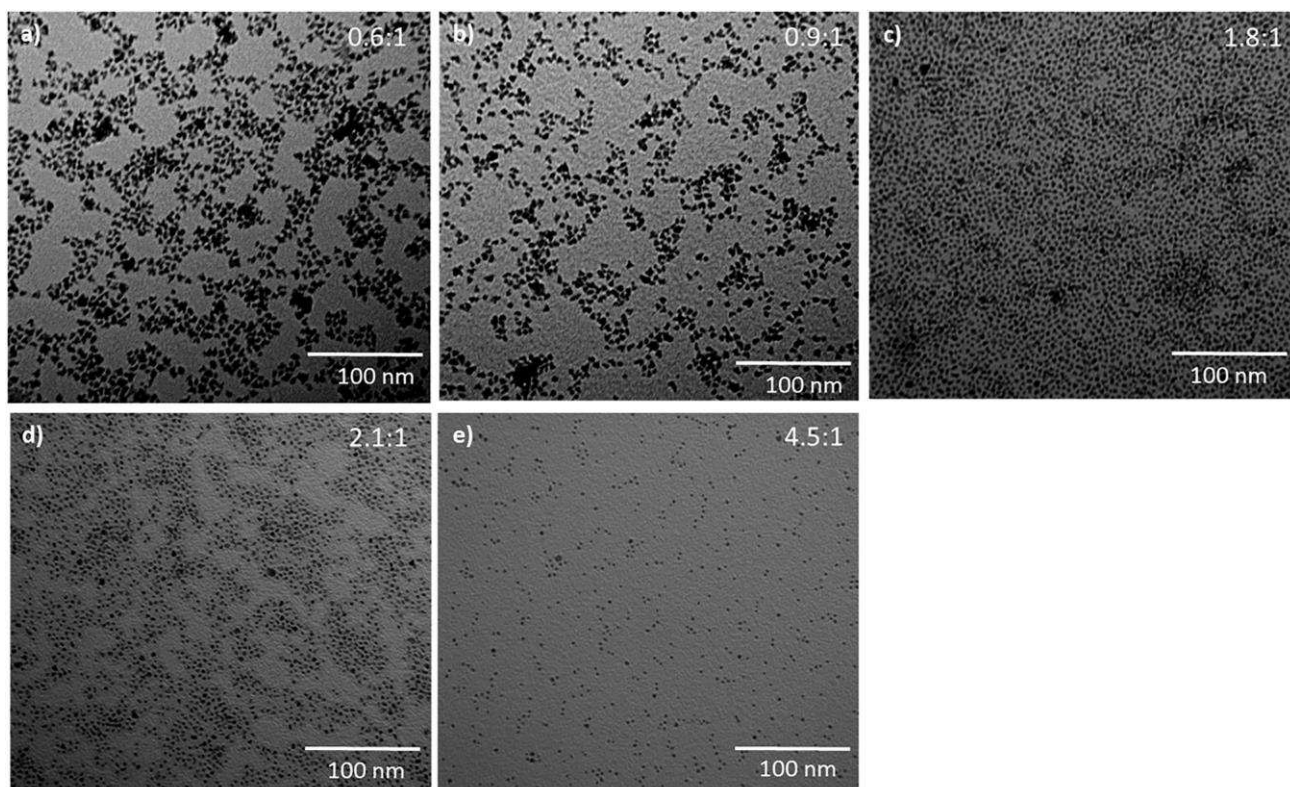


Figure 3 – Transmission electron micrographs showing PVP-Pt NPs synthesised with a) 0.6:1, b) 0.9:1, c) 1.8:1, d) 2.1:1, 4.5:1 molar ratio NaBH₄:H₂PtCl₆. Molar ratios are shown in top right corner of each image.

The nanoparticles synthesised from the three highest molar ratios of NaBH₄ to H₂PtCl₆, with the most uniform nanoparticles (figure 3c-e) were used as a stabiliser for producing PFOB-core polymer microcapsules. These nanoparticles were chosen for further investigation because as they were less disperse in size than the lower molar ratio samples, this should allow for a more homogeneous decoration of the polymer microcapsules. To standardise the number of nanoparticles added to the PVP used to stabilise the pre-microcapsule emulsion, the nanoparticles were dialysed in poly(ethylene glycol) (PEG) to concentrate the dispersion. The concentration of the nanoparticles after dialysis was 3.5×10^{14} ($\pm 0.1 \times 10^{14}$) NPs/mL. In each case, stable core-shell microcapsules were produced. Transmission electron micrographs in Figure 4 show apparent monolayer distributions of nanoparticles on the surface of the PLGA microcapsules in all three cases, and the surface coverage remains approximately 32% in all cases, calculated using ImageJ for 5 different capsules per sample (Table 1).

Table 1 – The effect of nanoparticle size on the surface coverage of PLGA microcapsules, and resulting gold shell thickness.

Nanoparticle size/nm	Average surface area covered/ %	Resulting gold shell thickness/nm
2.8	32.6 ± 9.0	106 ± 16

3.4	35.1 ± 1.4	105 ± 10
4.0	28 ± 2.8	109 ± 13

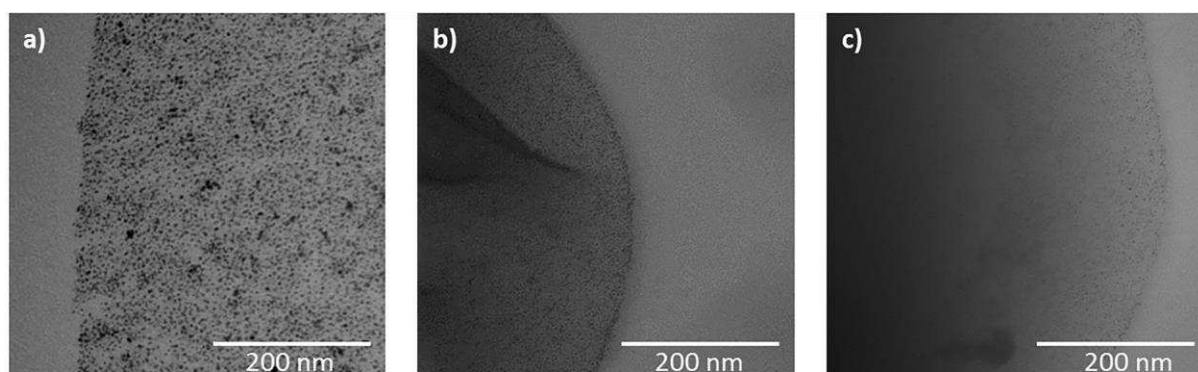


Figure 4 – Transmission electron micrographs showing representative areas of PLGA microcapsules with PVP-Pt NPs attached to the surface, where NP diameters of a) 4.0 nm , b) 3.5 nm , c) 2.8 nm , were used as the stabiliser.

Controlling gold shell morphology and thickness on PLGA microcapsules

As stable core-shell microcapsules were formed in all cases, the gold deposition was conducted on all three samples. Scanning electron micrographs in Figure 5 show that for the largest nanoparticles, approx. size of 4.0 nm, a full gold shell is deposited on the capsules (Figure 5a). The gold shells formed using the microcapsules decorated with the 3.5 nm diameter Pt nanoparticles appear to be slightly incomplete, as a number of pinholes are evident in Figure 5b (inset). When the smaller (2.8 nm) nanoparticles are used however, the coating begins to show some severe defects, with patchy coverage evident on some of the capsules, where the darker areas indicate exposed polymer (Figure 5c inset). Higher magnification images to further show the differences in shell quality as a function of nanoparticle size can be found in supplementary information, Figure S3.

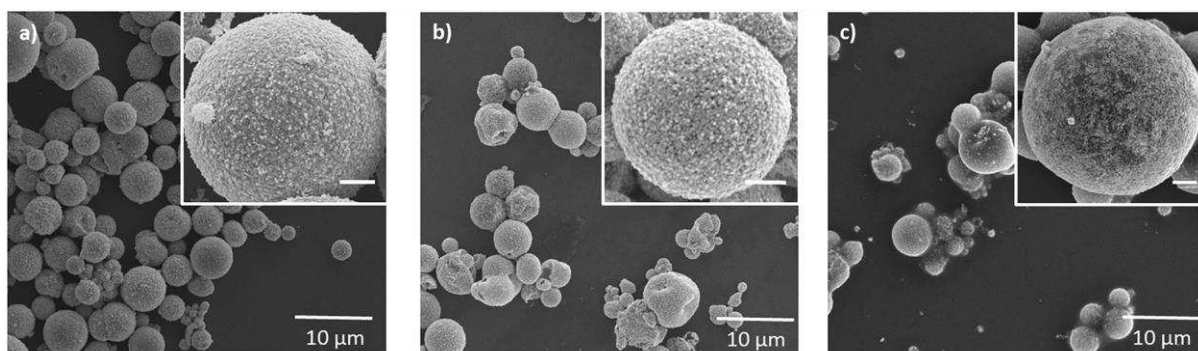


Figure 5 – Scanning electron micrographs showing the resulting gold shell when a) 4.0 nm b) 3.5 nm and c) 2.8 nm diameter nanoparticles were used to stabilise PLGA microcapsules. Insets show magnified images to demonstrate shell quality for each sample (scale bars for insets = 1 µm).

The mean shell thickness of each sample was measured using microtomy and image analysis (Table 1), as described previously.¹⁶ In the case where an incomplete shell was formed, the complete sections of the shell were used to calculate the overall shell thickness. Interestingly, although the 2.8 nm nanoparticles gave poorer quality gold coverage, in the areas where shells were produced and measurable, there was no significant difference in shell thickness as compared to the fully formed shells which were grown on the capsules with the 4.0 nm nanoparticles on the surface. This suggests that the size of the nanoparticle does not affect shell thickness, however it does affect the quality of the resulting shell. It is possible that as the nanoparticles become smaller they become less efficient as catalysts for the reduction of the gold salt, potentially due to the increase in PVP per unit surface area of nanoparticle blocking the catalytic sites. Alternatively, it is also possible that volume ratio of the nanoparticles engulfed by the polymer shell of the microcapsule plays an important role, with the smaller nanoparticles potentially exposing less catalytic surface to be used for the electroless deposition process as compared to their larger counterparts.

Controlling the gold shell thickness

Despite achieving a monolayer coverage of nanoparticles on the polymer capsule surface, the minimum shell thickness achieved using this new method was 110 ± 13 nm, which is not an improvement on that reported previously, when the nanoparticle layer expanded to more than a single monolayer.²¹ As we have noted, it is important to obtain the thinnest shells possible in order to produce the most cost-effective microcapsules, especially when using precious metals such as gold.

In an attempt to further improve our approach, the concentration of gold salt added to a known volume of microcapsules was systematically reduced from the original concentration of 40 mM. This part of our work was conducted on the capsules produced using 4.0 nm diameter nanoparticles, because this gave complete gold shells using a gold salt concentration of 40 mM. As the gold salt concentration was reduced, a decrease in the mean shell thickness was observed. The SEM 3View was used to generate cross-sections where microtome slices are cut from a resin block in which the sample is embedded, and then the remaining block face is imaged by SEM in situ. This eliminates problems associated with the resin slices tearing as they are removed from the block, as the block face is imaged rather than the removed slice. Using this method, 500 slices were taken from each sample and the images

were stacked to give a 3D reconstruction of the capsules. A movie of the reconstruction is included in the supplementary information. The centre-point, and thus thinnest part of the shell, is easily found from this reconstruction, allowing for the shell thickness to be measured at the equator of the sphere, thus reducing the error associated with our previous method of plotting a frequency curve of all the thicknesses from any part of the shell.^{16, 21} However, performing this analysis manually is extremely time consuming and relies on the assumption that the shell thickness is consistent, because only five measurements were taken per capsule. An automated analysis technique was developed using MATLAB, whereby each 3View section was converted to a binary image and subjected to a Euclidean distance transform. The thickness of the entire shell was measured as the minimum distance from the centre of the shell to the background and reported as an average value for that entire slice of the capsule. This was measured on individual capsules, slice by slice, to find the centre-point/thinnest part of the shell. There are two sets of data included in Figure 6, the orange circles represent the shell thickness measured manually across all the capsules in the sample window while the blue circles represent the shell thickness measured using MATLAB. A linear increase in shell thickness with gold concentration is apparent and this suggests that the deposition of more gold is limited only by the reaction time of 5 minutes. The thinnest shell was achieved using 2 mM of gold salt which was expected, and it was measured to be 56 nm using our automated process, and 40 nm by manual analysis. The manual results, whilst indicating thinner shells in all cases are within error of the automated results. The largest discrepancy occurs for 40 mM of gold salt, where the thickest shells are produced, and this is a result of the uneven surfaces of these thicker shells which increases the bias of a manual analysis because 5 random points are used per capsule to measure the thickness. It is important to note that the thinnest shells (56 nm) do not allow for any release of PFOB into chloroform, as shown by the absence of PFOB peaks in the NMR spectra from the release studies (Figure S1). This confirms that the metal shells grown in this case are indeed impermeable, as seen for different core materials in our previous works.^{16, 21, 31}

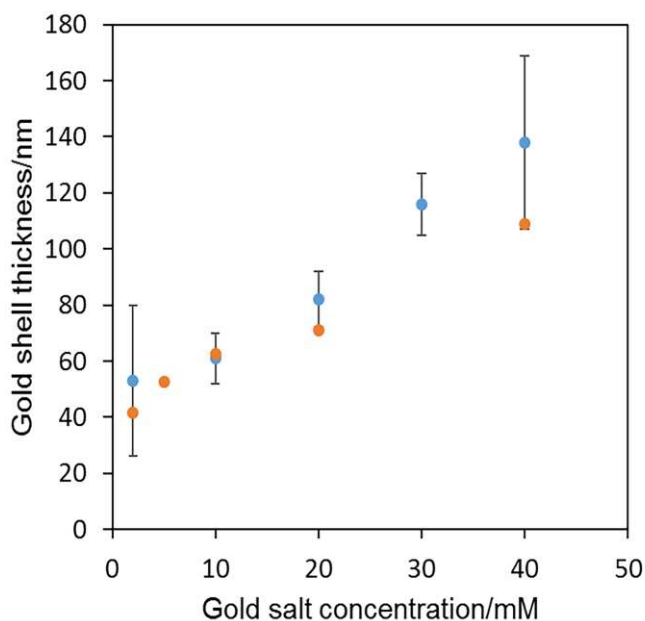


Figure 6 – Relationship between gold salt concentration used in electroless deposition process and resulting metal shell thickness on PLGA microcapsules, blue circles – Matlab automated analysis method, orange circles – manual image analysis method.

The surface morphology of the gold shells appears smoother as the gold salt concentration is reduced (Figure 7) and this is consistent with less gold attaching to the surface and thus the thinner films we observe at the lower concentrations. One possible explanation for this is that the gold shells formed with lower salt concentrations grow more slowly, due to the longer diffusion times required for the ions to reach the catalytic nanoparticle sites. This slower growth is likely to result in more even and continuous films. Higher magnification images to further show the differences in shell roughness as a function of nanoparticle size can be found in supplementary information, Figure S4.

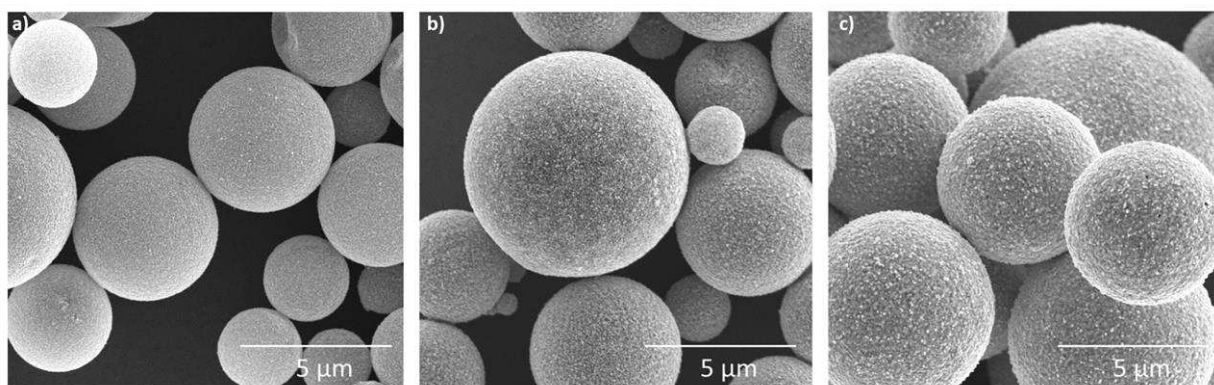


Figure 7 – Scanning electron micrographs showing gold shell microcapsule surfaces becoming increasingly rough as the amount of gold salt, and thus shell thickness increases, a) 5 mM, b) 10 mM and c) 40 mM H[AuCl₄] used for electroless deposition.

Conclusions

We have developed a novel method by which polymeric microcapsules can be synthesised using a combination of PVP-Pt nanoparticles and PVP as stabilisers. We found that during the polymer shell formation, PVP-Pt nanoparticles become immobilised on the surface of the polymer, and can then be used as catalytic loci for electroless deposition of gold shells, resulting in a simplified technique for creating metal shell microcapsules compared to previous methods.^{16,31} A relationship has been established between the molar ratio of reducing agent to platinum salt and the size of the resulting NPs, where lower amounts of reducing agent resulted in larger particles which showed signs of aggregation. The size of NPs had no significant effect on shell thickness, but was found to affect the quality of the resulting gold shells, with the smaller NPs producing incomplete shells. Importantly, by reducing the concentration of gold salt available for electroless deposition we have successfully produced PLGA microcapsules with more cost effective gold shells, as thin as 56 ± 13 nm, which are capable of full core retention. Due to the ability to fully retain an active core, the biocompatible microcapsules with an impermeable shell of controllable thickness described here have significant potential as drug delivery devices. Furthermore, the ability to fully retain the echogenic core of PFOB oil offers the potential for the development of highly stable ultrasound contrast agents.

Acknowledgements

The authors acknowledge the University of Queensland for the award of an Early Career Researcher Grant to ALT to enable this work to be conducted. We also acknowledge the facilities, and the scientific and technical assistance, of the Australian Microscopy & Microanalysis Research Facility at the Centre for Microscopy and Microanalysis, The University of Queensland, and we specifically thank Dr Robyn Webb for running the SEM 3view. This work was performed in part at the Queensland node of the Australian National Fabrication Facility (ANFF).

References

1. S. Ray, U. Raychaudhuri and R. Chakraborty, *Food Bioscience*, 2016, **13**, 76-83.
2. M. Esther Gil-Alegre, I. Gonzalez-Alvarez, L. Gutierrez-Pauls and A. I. Torres-Suarez, *J Microencapsul*, 2008, **25**, 561-568.
3. M. Iqbal, N. Zafar, H. Fessi and A. Elaissari, *Int J Pharm*, 2015, **496**, 173-190.
4. M. X. L. Tan and M. K. Danquah, *Chemical Engineering & Technology*, 2012, **35**, 618-626.
5. Z. Zhang and S. S. Feng, *Biomaterials*, 2006, **27**, 4025-4033.

6. M. Badila, C. Brochon, A. Hebraud and G. Hadziioannou, *Polymer*, 2008, **49**, 4529-4533.
7. S. Leelajariyakul, H. Noguchi and S. Kiatkamjornwong, *Progress in Organic Coatings*, 2008, **62**, 145-161.
8. B. J. Park, S. Y. Hong, H. H. Sim, H. J. Choi and Y. S. Yoon, *Materials Chemistry and Physics*, 2012, **135**, 259-263.
9. P. H. Keen, N. K. Slater and A. F. Routh, *Langmuir*, 2014, **30**, 1939-1948.
10. M. Yilmaz and A. Kati, *Cellulose*, 2015, **22**, 4077-4085.
11. C. Quellet, M. Schudel and R. Ringgenberg, *Chimia*, 2001, **55**, 421-428.
12. A. L. Tasker, J. P. Hitchcock, L. He, E. A. Baxter, S. Biggs and O. J. Cayre, *Journal of colloid and interface science*, 2016, **484**, 10-16.
13. A. Ammala, *Int J Cosmet Sci*, 2013, **35**, 113-124.
14. P. J. Dowding, R. Atkin, B. Vincent and P. Bouillot, *Langmuir*, 2005, **21**, 5278-5284.
15. P. J. Dowding, R. Atkin, B. Vincent and P. Bouillot, *Langmuir*, 2004, **20**, 11374-11379.
16. J. P. Hitchcock, A. L. Tasker, E. A. Baxter, S. Biggs and O. J. Cayre, *ACS Appl Mater Interfaces*, 2015, **7**, 14808-14815.
17. M. A. Zieringer, N. J. Carroll, A. Abbaspourrad, S. A. Koehler and D. A. Weitz, *Small*, 2015, **11**, 2903-2909.
18. H. Lee, C. H. Choi, A. Abbaspourrad, C. Wesner, M. Caggioni, T. Zhu and D. A. Weitz, *ACS Appl Mater Interfaces*, 2016, **8**, 4007-4013.
19. C. Sun, K. Shu, W. Wang, Z. Ye, T. Liu, Y. Gao, H. Zheng, G. He and Y. Yin, *Int J Pharm*, 2014, **463**, 108-114.
20. Q. Sun and A. F. Routh, *European Polymer Journal*, 2016, **77**, 155-163.
21. A. L. Tasker, J. Hitchcock, E. A. Baxter, D. O. J. Cayre and S. Biggs, *Chem Asian J*, 2017, **12**, 1641-1648.
22. A. Loxley and B. Vincent, *Journal of colloid and interface science*, 1998, **208**, 49-62.
23. S. Horiuchi and Y. Nakao, *Surface & Coatings Technology*, 2010, **204**, 3811-3817.
24. O. J. Cayre and S. Biggs, *Journal of Materials Chemistry*, 2009, **19**, 2724-2728.
25. T. Feczko, J. Toth and J. Gyenis, *Colloids and Surfaces a-Physicochemical and Engineering Aspects*, 2008, **319**, 188-195.
26. E. Pisani, E. Fattal, J. Paris, C. Ringard, V. Rosilio and N. Tsapis, *Journal of colloid and interface science*, 2008, **326**, 66-71.
27. O. Diou, A. Brulet, G. Pehau-Arnaudet, E. Morvan, R. Berti, K. Astafyeva, N. Taulier, E. Fattal and N. Tsapis, *Colloids Surf B Biointerfaces*, 2016, **146**, 762-769.
28. O. Diou, N. Tsapis, C. Giraudeau, J. Valette, C. Gueutin, F. Bourasset, S. Zanna, C. Vauthier and E. Fattal, *Biomaterials*, 2012, **33**, 5593-5602.
29. C. A. Schneider, W. S. Rasband and K. W. Eliceiri, *Nat Methods*, 2012, **9**, 671-675.
30. R. P. Seekell, A. T. Lock, Y. Peng, A. R. Cole, D. A. Perry, J. N. Kheir and B. D. Polizzotti, *Proceedings of the National Academy of Sciences*, 2016, **113**, 12380-12385.
31. J. P. Hitchcock, A. L. Tasker, K. Stark, A. Leeson, E. A. Baxter, S. Biggs and O. J. Cayre, *Langmuir*, 2018, **34**, 1473-1480.